

Memory effects govern scale-free dynamics beyond universality classes

K. Duplat,¹ A. Douin,¹ and O. Ramos^{1,*}

¹*Institut Lumière Matière, UMR5306 Université Lyon 1-CNRS, Université de Lyon 69622 Villeurbanne, France.*

(Dated: February 3, 2026)

Scale-invariant avalanches –with events of all sizes following power-law distributions– are considered critical. Above the upper critical dimension of four, the mean-field solution with a robust $3/2$ size exponent describes the dynamics. In two and three dimensions, spatial constraints yield smaller yet robust exponent values governed by universality classes. However, both earthquake data and experiments often show exponent values larger than $3/2$, challenging those theoretical arguments based on critical behavior. Through extensive simulations in the classical OFC earthquake model, here we show a clear transition from the theoretical expected behavior of a robust exponent value, to a regime of quasi-critical dynamics with larger than $3/2$ exponents that depend on dissipation. While the first critical regime exhibits an inherently memoryless behavior, both the transition and the second regime are driven by memory effects provoked by the growth of avalanches over the traces left by previous events, due to dissipative mechanisms. The system hovers at a distance d_{cp} from the critical point, and accounting for a power-law distribution of d_{cp} , validated by susceptibility measurements, captures the transition. This framework provides a unified description of both critical and quasi-critical behavior, and thus of the full spectrum of scale-free dynamics observed in nature.

I. INTRODUCTION

In many slowly driven systems, including earthquakes [1–3], granular faults [4–7], sandpiles [8, 9], and subcritical rupture [10–14], energy accumulates gradually and is released through sudden events spanning a wide range of sizes, typically following power-law distributions. The consideration of a critical point as an attractor of the dynamics, introduced by the Self-Organized Criticality (SOC) [15, 16] in 1987, established a direct link between scale-free avalanches and phase transitions [17]. Following this path, the mapping of avalanche dynamics onto a branching process in a Bethe lattice [18] set the mean-field (MF) expectation of the size distribution of the events $P(s) \sim s^{-\tau} \exp(-s/\lambda)$, with $\tau = 3/2$ and λ scaling with system size. Scale-free avalanches spanning the system mark criticality [19], while dissipation shifts the cut-off λ to smaller values, destroying it. Yet, the MF exponent $\tau = 3/2$ remains remarkably robust [19–22].

In Bethe lattices and MF approximations, the absence of spatial constraints renders the dynamics equivalent to infinite-dimensional systems. Below the upper critical dimension (UCD), loop formation during avalanche propagation complicates analytical treatment [30]. Over two decades, numerous studies have sought to determine exponent values and classify avalanches into universality classes [19–26, 30, 31]. Zhang’s 1989 relation [23] $\tau = 2 - 2/d$, where d is the system dimension, implied UCD=4, a result refined by subsequent numerical [24, 25] and analytical [26] work (Fig. 1a). Despite model-dependent discrepancies, consensus holds that in two and three dimensions $\tau < 3/2$, as loops enhance local triggering and increase the likelihood of large avalanches. A major advance came in 2009 when Le Doussal and Wiese used the functional renormalization group to calculate exponents for various universality classes [21]. Their results are consistent with $\tau = 2 - 2/(d + \zeta)$, where ζ is the static roughness exponent of an elastic interface pinned by quenched disorder.

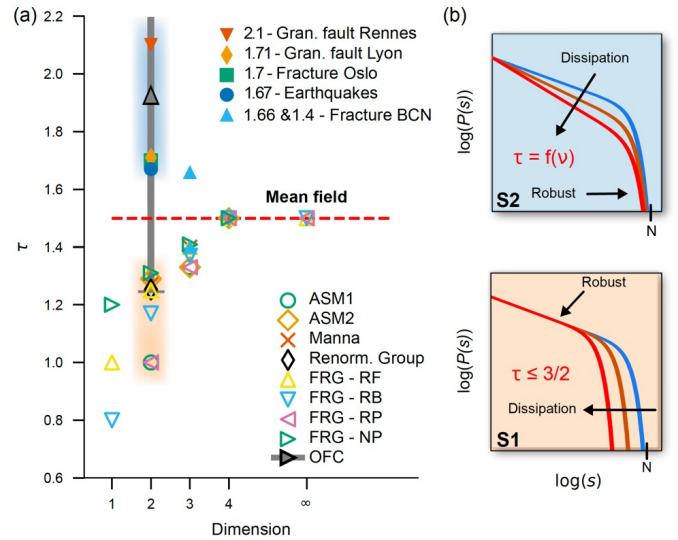


Figure 1. Two distinct behaviors. (a) (open symbols) Theoretical predictions of the exponent values τ of the avalanche size distribution in Abelian sandpile models (ASM1 [23] and ASM2 [24]), Manna model [25], Renormalization group [26] and Functional Renormalization Group (FRG) [21] with: Random field (RF), Random bond (RB), Random periodic (RP) and Non-periodic (NP). In UCD=4 and above, the MF solution of $3/2$ is obtained. For two- and three-dimensions exponent values cluster below the value $3/2$ in different universality classes. (solid symbols) OFC model and selection of experimental results in granular faults in Lyon [4] and Rennes [5] Labs, fracture in Oslo [27] and Barcelona (BCN) [11], and earthquake data [28, 29] displaying exponent values above $3/2$. (b) Sketch of the two distinct behaviors of the avalanche size distributions when submitted to dissipation. **S1**: robust $\tau \leq 3/2$ and cut-off s_{max} that retreats with dissipation. **S2**: robust cut-off s_{max} proportional to the system size N and τ values that increases with dissipation.

Under random periodic disorder, with $\zeta = 0$, their results matched Zhang’s prediction [23]. This confirmed $\tau = 3/2$ for $d \geq UCD$ and smaller values in lower dimensions (Fig. 1a).

* osvanny.ramos@univ-lyon1.fr

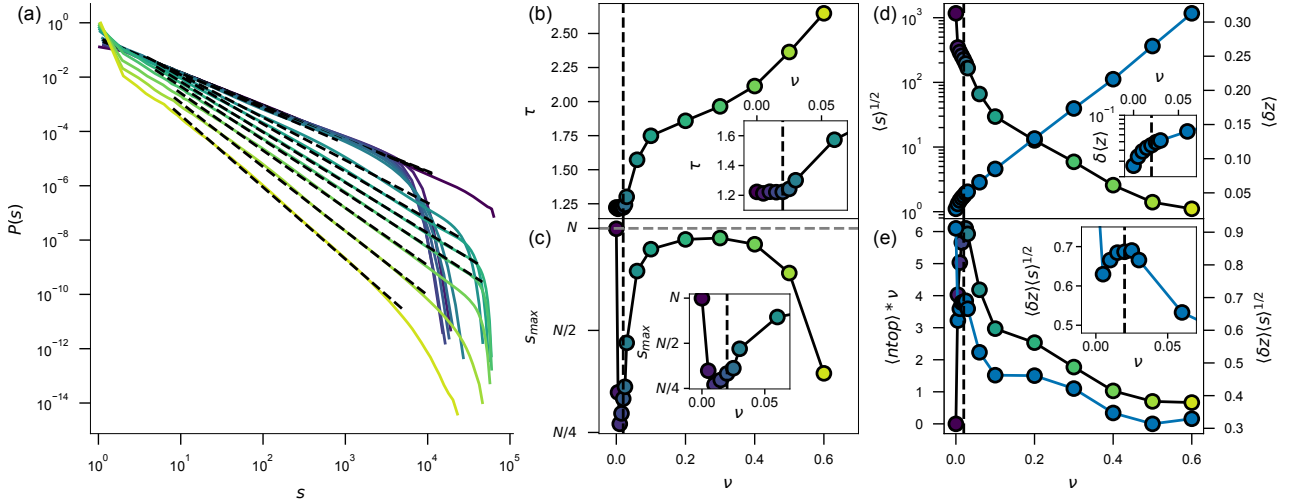


Figure 2. Size distributions & trace dependence. (a) Avalanche size distribution in the OFC model for different dissipation values ranging from 0 to 0.6 (dark to bright colors) for a system size $L = 256$. (b) Power law exponents from the dashed lines in (a) as a function of dissipation. A vertical dashed line at $\nu = 2\%$ marks the threshold beyond which the exponent begins to increase. All insets provide a zoom into the low dissipation region. (c) Maximum avalanche size as a function of dissipation. The horizontal dashed line is a visual indicator of the size of the system. (d) Average linear size of the avalanches $\langle s \rangle^{1/2}$, scaling with the perimeter of the traces (color gradient) and mean value of the thickness δz of the trace left by the avalanches (in blue). (e) Average dissipated energy, $\langle n_{top} \rangle \nu$, where $\langle n_{top} \rangle$ is the mean number of topplings as a function of dissipation (indicated by a color gradient). The graph matches that of the product $\langle \delta z \rangle \langle s \rangle^{1/2}$, (in blue) indicating a direct relationship between dissipation and the traces left by the avalanches.

We refer to these applications of the critical-transitions formalism, which yield robust $\tau \leq 3/2$ across dimensions, as the **S1** scenario (Fig. 1b).

The branching process [18] captures the essence of this behavior: avalanches propagate stochastically between neighboring sites until growth ceases, with each event occurring independently, under statistically identical conditions. The absence of correlations between avalanches makes prediction impossible, which was a central claim of SOC. This notion, however, sparked intense debate when applied to earthquakes [32–34]. In the 1990s, limited seismic and experimental data were not precise enough to confront and guide theoretical efforts. Today, high-quality earthquake catalogs reveal exponents around 1.67 [28, 29], while laboratory experiments consistently report $\tau > 3/2$ across many decades of energy release [4, 5, 9, 11, 27]. See Appendix A for details. Moreover, observed exponent values vary with experimental conditions [4, 5, 9, 11], challenging the universality predicted by classical SOC theory.

This enduring discrepancy between theoretical predictions capped at $\tau = 3/2$ and observations showing larger, non-universal exponents (Fig. 1a), highlights the need for a new unifying framework. Previous attempts to reconcile this gap, such as including relaxation mechanisms [35, 36] or fragmenting avalanches [37], produce aftershock sequences that alter the global exponent. Yet, such dual distributions for aftershocks and background activity are absent in both experiments and natural seismicity [38].

Consistent with observations, the classical Olami-Feder-Christensen (OFC) model of earthquakes [39, 40] yields $\tau >$

$3/2$ values that vary with dissipation. We identify these dynamics with τ values larger than the predicted in the **S1** scenario –which in general are not robust– as the **S2** scenario (Fig. 1b). Here we show that, for very low dissipation values, the OFC model also exhibits an unexplored **S1**-type regime. The existence of distinct **S1** and **S2** regimes, together with the transition between them, offers a unique opportunity to develop a unified framework for understanding scale-free dynamics across driven systems.

II. SIMULATIONS IN THE OFC MODEL

We performed extensive numerical simulations of the Olami–Feder–Christensen (OFC) model [39], defined on a square lattice of $N = L \times L$ sites with open boundary conditions. Each site i is initialized with a random value $z_i \in [0, 1]$ and a common threshold $z_{\text{th}} \equiv 1$. At each loading step, the system is uniformly driven by the minimal increment $\Delta z = z_{\text{th}} - z_{\text{max}}$, where z_{max} is the site closest to the threshold, ensuring that only one site becomes unstable at a time.

When a site reaches the threshold, it topples: its value is reset to zero and a fraction α of its energy is equally redistributed to its four nearest neighbors. The coupling parameter $\alpha \in [0, 1/4]$ controls the dissipation in the system, quantified by $\nu = 1 - 4\alpha$, with $\alpha = 1/4$ corresponding to conservative bulk dynamics and $\alpha = 0$ yielding trivial periodic behavior [41]. A toppling may trigger further instabilities, leading to a cascade that continues until all sites satisfy $z_i < z_{\text{th}}$, defining an avalanche. To preserve the temporal structure of

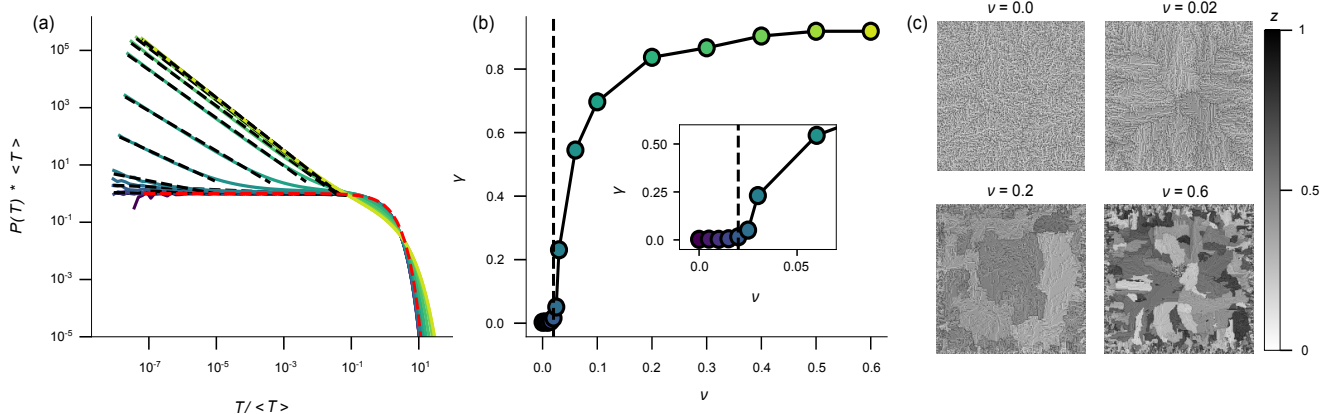


Figure 3. Memory effects & patch formation. (a) Inter-event time distribution normalized by the mean intertime $\langle T \rangle$, for different dissipation values ranging from 0 to 0.6 (dark to bright colors), in a system of size $L = 256$. The black dashed line represent power law fits for each dissipation value, while the red dashed line correspond to a pure exponential decay. (b) Exponent γ of the power law fit from (a) as function of the dissipation. The inset provides a zoomed-in view of the low dissipation region. The vertical dashed line is a visual indicator for 2% dissipation. Below 2% distributions show a pure exponential decay, indicating a memoryless Poisson process, while above the transition, memory effects linked to temporal clustering of events, increased monotonically with dissipation. (c) Patches of neighboring z -values show an increase in contrast and a decrease in size with dissipation above the transition.

avalanches, a parallel updating scheme is employed [42]. The avalanche size s is defined as the number of distinct sites that topple, regardless of how many times each site topples.

Inter-event times T are identified with the loading increments Δz , while avalanche durations are neglected. To ensure stationarity, an initial transient was discarded, ranging from 10^5 avalanches for $\nu = 0$ up to 2×10^{11} avalanches for $\nu = 0.60$. Depending on the dissipation, the total number of simulated avalanches varied between 10^8 and 10^{13} . The simulations required approximately 15 months of computation on a local server to obtain the statistics reported in Figs. 2 and 3.

III. DIFFERENT REGIMES IN AVALANCHE DYNAMICS

Figure 2a shows the avalanche size distribution for a system of size $L = 256$ after reaching a stationary state. In the conservative case ($\nu = 0$) and at very low dissipation levels $\nu < 2\%$, we obtain a robust exponent of $\tau_c \simeq 1.22$ (Fig. 2b), while a cut-off, defined as the maximum avalanche size s_{max} , retreats with increasing dissipation (Fig. 2c) consistent with the **S1** scenario of Fig. 1b. Beyond 2% dissipation, the exponent increases and the cut-off gradually approaches the size of the system, transitioning to the **S2** scenario. Simulations at different system sizes (Appendix A, Fig. 7) confirm the fact that $s_{max} \simeq N$ over the whole interval $\nu = 0.1 - 0.4$. At higher dissipation values, the statistics is not sufficient in order to obtain clear cut-off values.

Is the physics of this **S1** regime equivalent to that of a branching process on a Bethe lattice [18], described earlier? A key distinction is that in the OFC model, avalanches evolve over the *traces* left by previous events, potentially inducing

temporal correlations between them. However, Fig. 3 shows that, in the **S1** regime, inter-event times follow a memoryless Poisson process [43]. This behavior arises because the *trace thickness*, defined as $\delta z \equiv |\langle z_i \rangle_{i \in A} - \langle z_i \rangle_{i \notin A}|$, with A denoting the sites involved in the most recent event, remains very small below 2% dissipation (inset, Fig. 2d). Consequently, avalanches in the **S1** regime display a wave-like behavior, with traces too thin to induce memory effects in the time series. Memory effects, defined as deviations from a Poissonian inter-event time distribution [43] (Fig. 3a,b), are therefore absent, indicating that **S1** dynamics are inherently memoryless.

IV. MEMORY EFFECTS GOVERN THE **S2** REGIME

The propagation of the avalanches creates a rim at its *perimeter*, scaling as $\langle s \rangle^{1/2}$, which is often a triggering point for new events. As dissipation increases, $\langle \delta z \rangle$ increases sharply between 0 and 2% dissipation (inset, Fig. 2d). This rise outweighs (except in the conservative case) the decrease in $\langle s \rangle^{1/2}$ producing a maximum in $\langle \delta z \rangle \langle s \rangle^{1/2}$ at 2% dissipation (Fig. 2e), where we identify the transition between **S1** and **S2** regimes. $\langle \delta z \rangle \langle s \rangle^{1/2}$ defines a *boundary layer* of the traces that combines both thickness and rim contributions. This boundary layer follows the same trend as the mean dissipated energy $\langle n_{top} \rangle \nu$ (Fig. 2e). This indicates a direct relation between the energy dissipated and the trace left by the avalanches, both having a maximum that coincides with the emergence of memory effects [43–45]. In the conservative case of $\nu = 0$, where $\langle \delta z \rangle \langle s \rangle^{1/2}$ shows its highest value, traces are very extended, but also very shallow, provoking no memory effects in the dynamics. A visual signature of the

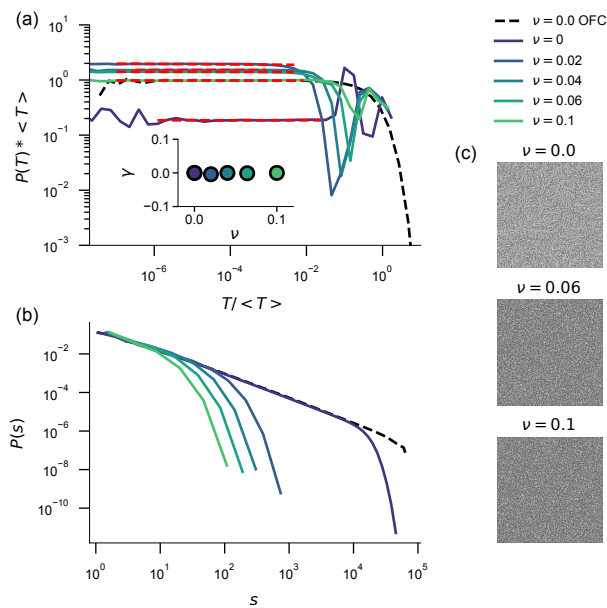


Figure 4. Democratic algorithm. (a) Inter-event time distribution normalized by the mean inter-event time $\langle T \rangle$ for different dissipation values. The distribution for the conservative case in the non-modified OFC model (dashed line) is also plot for comparison. (b) Avalanche size distribution. A **S1** behavior –with a robust $\tau = \tau_c \simeq 1.22$ and a cut-off that retreats with dissipation– is obtained. (c) Snapshots of the structure under different dissipation values show that no patches appear.

traces is the formation and evolution of patches in the structure [46], that appear only in the **S2** regime (Fig. 3c).

To disentangle the respective roles of dissipation and memory in the **S1–S2** transition, we modified the OFC dynamics by implementing a *democratic* triggering algorithm. Instead of selecting the most unstable site, the trigger site is chosen at random and forced to topple by setting its value to $z = 1$. After the resulting avalanche terminates, a new random site is selected and the procedure is repeated. This protocol removes temporal correlations between consecutive events, thereby suppressing memory effects while preserving the redistribution rules and spatial constraints of the model (Fig. 4a).

Under these conditions, the system systematically exhibits **S1**-type behavior, characterized by a robust avalanche-size exponent $\tau_c \simeq 1.22$, identical to that of the conservative OFC model. The avalanche cut-off continues to shift with dissipation, with no indication of a transition (Fig. 4b). Moreover, because avalanches do not evolve on traces left by previous events, no spatial organization in the form of persistent traces or patches develops (Fig. 4c). These results demonstrate that dissipation alone is insufficient to produce the **S1–S2** transition, and that memory effects, mediated by traces, are essential.

While dissipation destroys criticality in the classical **S1** scenario (Fig. 1b), its gradual increase –under the natural constraint that avalanches develop over the traces left by previous

events– progressively amplifies these imprints until a threshold is reached, where memory effects emerge (Fig. 3), signaling the transition to the **S2** regime. As a result, criticality is recovered, defined here by the occurrence of events that span the entire system ($s_{max} \simeq N$). However, as energy is lost, the mean avalanche size decreases with dissipation. Because the scale-free character of the distribution is preserved, the exponent τ necessarily increases, making system-spanning events increasingly rare. To understand how this scale-free organization persists despite dissipation, we first examine the critical properties of the system in the **S2** regime.

V. CRITICAL BEHAVIOR REVISITED

Using the standard definition of criticality, whereby the largest avalanche scales with system size ($s_{max} \simeq N$), the introduction of dissipation in the OFC model first abruptly destroys criticality (**S1** regime), then progressively rebuilds it across the **S1–S2** transition, and finally restores it in the **S2** regime, albeit with a different exponent and, consequently, altered dynamical properties. This conventional definition, rooted in the **S1** scenario, implicitly assumes that the system is in a state where, *at any moment, a small avalanche can cascade into a system-spanning event*. We identify this property as the *criticality criterium* (CC), which captures the intrinsic fluctuation-dominated nature of truly critical systems [17, 47, 48].

To test whether the CC is fulfilled, we introduce a *maximum susceptibility* protocol $\chi_{max}(\nu)$, designed to measure the largest possible avalanche size $s_c(\nu)$ accessible from a given configuration. For a fixed snapshot of the system evolving under dissipation ν , the system is first uniformly loaded by $\Delta z = z_{th} - z_{max}$. Then, starting from the same configuration, sites are sequentially forced to topple, each generating an avalanche of size s_i under the standard redistribution rules. The maximum achievable avalanche size is defined as $s_c(\nu) = \max(s_i)$. We verified that forcing a random subset of 10% of sites, excluding the most unstable one, yields equivalent results, and this reduced protocol is therefore adopted.

We apply this analysis to ensembles of 5000 randomly selected configurations for each dissipation value: half taken immediately before a large event ($s_{next} \geq N/4$), and half preceding a single-site event ($s_{next} = 1$) and temporally distant from large avalanches, i.e., no large event before a $\langle T \rangle/2$ time interval, and after a $\langle T \rangle/4$ time interval from the event. A configuration is said to satisfy the CC if $s_c \geq N/4$, meaning that an arbitrarily small perturbation can trigger a system-spanning event.

In the conservative case ($\nu = 0$), the CC is fulfilled in essentially all configurations: system-spanning avalanches can be generated with probability 100% before large events and approximately 98% even when the next event is minimal (Fig. 5a). The system is therefore permanently critical. In contrast, in the **S2** regime, configurations preceding small events are typically unable to generate large avalanches. The probability of satisfying the CC drops to about 20% immediately after the transition and vanishes as dissipation increases (Fig. 5a). Thus, although large avalanches still occur in the

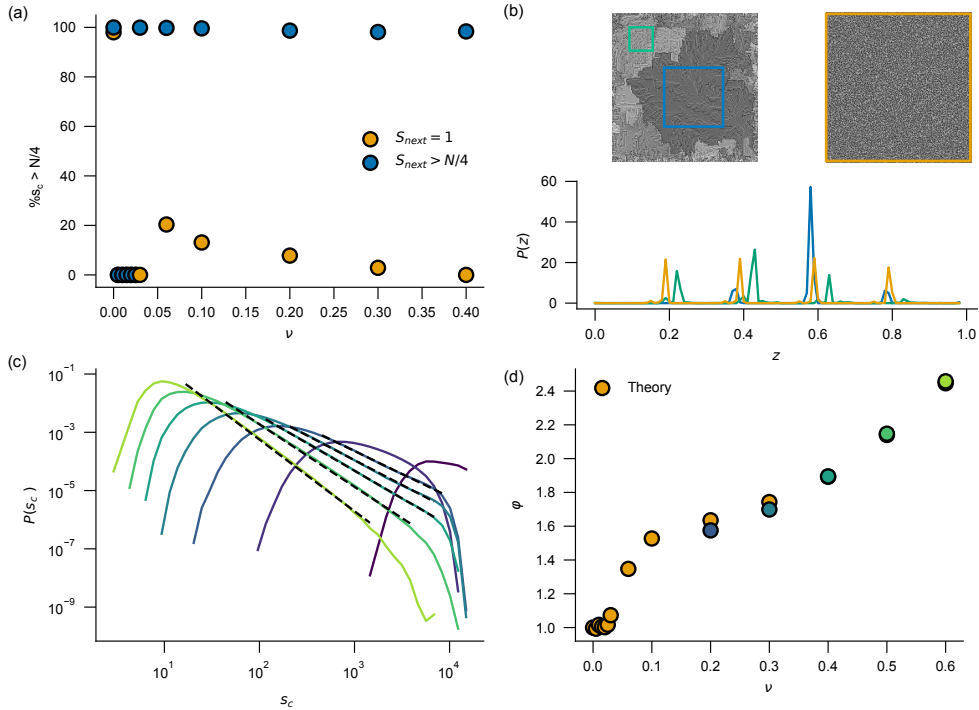


Figure 5. Transiting from critical to quasi-critical behavior. (a) Percentage of $s_c(\nu) \geq N/4$ for configurations immediately preceding large events ($s_{next} \geq N/4$), and those preceding very small events ($s_{next} = 1$) that are also far in time from any large event. For $\nu = 0$, large avalanches can be triggered from both types of configurations, indicating critical behavior. In contrast, for high dissipation values (**S2** scenario), the percentage of $s_{next} = 1$ configurations is about 20% just after the transition and then decreases monotonically to zero as dissipation increases. (b) For a given dissipation $\nu = 0.2$, the distribution of z -values –containing four peaks separated by α – is similar inside the patches (left panel) and in the case of one single domain (right panel), corresponding to a distribution of events with exponent $\tau_c \simeq 1.22$ in the democratic algorithm, suggesting a common intrinsic dynamics. (c) Distributions of s_c for different dissipation values ranging from 0 to 0.6 (dark to bright colors). They follow power laws for large dissipation values. (d) Power-law exponents from the dashed lines in (c) as a function of dissipation (colors). Theoretical points correspond to $\varphi(\nu) = \tau(\nu) - \tau_c + 1$, giving the expected behavior in the OFC model.

S2 regime, the system is not *permanently* critical. Instead, it hovers around the critical point [48], briefly entering a critical state only prior to system-spanning events [49, 50], an instance of *quasi-* or *near-criticality* [48, 51].

VI. QUASI-CRITICALITY AND CHANGE IN EXPONENT VALUES

Here we show with a simple model how hovering around the critical point can modify the exponent of a power-law distribution, enabling a transition from the critical dynamics with $\tau = \tau_c$ to any particular larger exponent value. Consider a system exhibiting avalanches whose size distribution follows

$$P(s) = s^{-\tau_c} e^{-s/s_c} \quad (1)$$

where τ_c is the size exponent, and s_c is the cut-off. The system is strictly critical only in the limit $s_c \rightarrow \infty$, which corresponds to $s_c \rightarrow N$ in the OFC model with dissipation $\nu = 0$. Introducing dissipation reduces s_c and –in the absence of memory effects, as shown in the democratic algorithm– the exponent remains robust (Fig. 4). Traces partition the system into patches whose boundaries act as natural barriers to

avalanches. The internal structure of each patch is identical to that of a memoryless system –obtained in the democratic algorithm– but with the same level of dissipation (Fig. 5b). Only small shifts in the z -distributions distinguish different patches. This suggest that inside each patch, Eq. (1) may describe the dynamics, rescaled down by the patch size. Furthermore, within each configuration or snapshot of the dynamics, Eq. (1) may also apply, with the cut-off s_c corresponding to the maximum avalanche size allowed in that specific configuration.

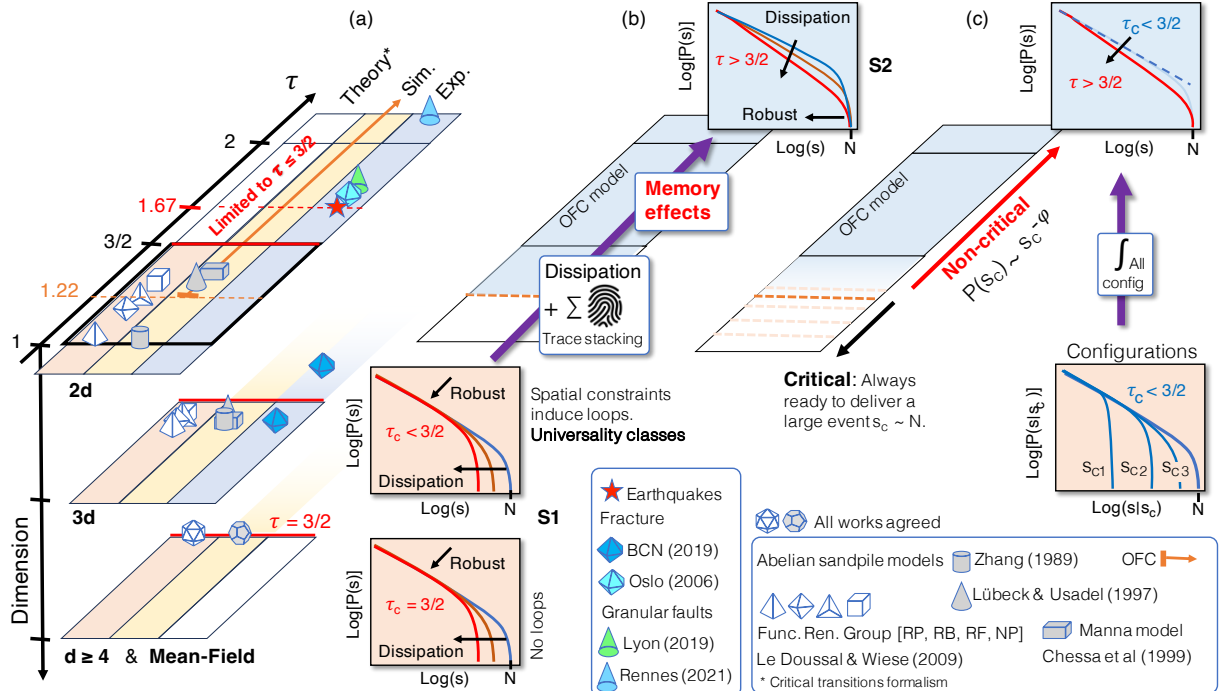
Let us assume that the cut-off values are distributed as $P(s_c) \sim s_c^{-\varphi}$. We can then define a distance to the critical point (CP) as $d_{cp} \equiv 1/s_c$. This change in variables results in:

$$P(d_{cp}) = d_{cp}^{-\gamma} \mathcal{L}(d_{cp}), \quad (2)$$

with $\gamma = 2 - \varphi < 1$

where we have added $\mathcal{L}(d_{cp})$, a slowly varying function near the origin. Thus, the system hovers at a distance d_{cp} from the CP, reflecting its dynamical trajectory through configurations characterized by different values of s_c .

Stacking the traces that, above a threshold, generate memory effects, can be modelled as integrating over the different



presses criticality by reducing the cut-off of the size distribution.

In contrast, the **S2** regime emerges from the interplay between dissipation and avalanche stacking (Fig. 6b). Avalanche traces grow until they reach a threshold at which memory effects appear. The resulting buildup of stress and structural organization occasionally permits large, system-spanning events ($s_{max} \simeq N$), restoring a scale-free size distribution. These extreme avalanches, however, become increasingly rare as dissipation grows, so the system never fully regains criticality but instead hovers around the critical point.

Assuming –and validating it within the OFC model– a power-law distribution of hovering distances, $P(d_{cp}) = d_{cp}^{-\gamma}$, accounts for the transition from **S1** critical dynamics with exponent τ_c to **S2** quasi-critical dynamics (Fig. 6c) with $\tau(\nu) = \tau_c + 1 - \gamma(\nu)$. This framework provides a plausible explanation for the emergence of scale-free dynamics with $\tau > 3/2$ in nature.

In real systems, avalanches occur sequentially, with each event influenced by the traces left by its predecessors. Memory effects therefore arise naturally from this trace dependence, an intrinsic feature of driven dissipative systems. Such effects govern the dynamics not only in systems with dynamic disorder, such as tectonic or granular faults, but also in systems with quenched disorder, as observed in fracture experiments.

ACKNOWLEDGMENTS

We acknowledge François Detcheverry for the original idea of the theoretical development and Kay Wiesse, Andrei Fedorenko, Ezequiel Ferrero, Nicolas Bain and Olivier Cochet-Escartin for helpful discussions. This work was supported by the ANR grant ANR-22-CE30-0046

The authors declare that they have no competing interest.

DATA AVAILABILITY

All data present in the manuscript and are also available at Figshare: <https://doi.org/10.6084/m9.figshare.30784430>

AVALANCHE DEFINITION AND FINITE SIZE SCALINGS

In the context of critical phenomena, the standard definition of the size of an event is given by its volume [21, 39, 57] (in an n -dimensional space). Accordingly, to meaningfully compare scale-invariant avalanches with critical phenomena, *the avalanche size must be proportional to the avalanche volume* [28].

For earthquakes, the appropriate definition of avalanche size is the seismic moment $M_0 = \mu Sd$, which is proportional to the released elastic energy [28].

Earthquake analogue experiments. In laboratory settings, the radiated acoustic seismic energy [58], $E_s = 1.6 \times 10^{-5} M_0$, scales linearly with M_0 and therefore provides an

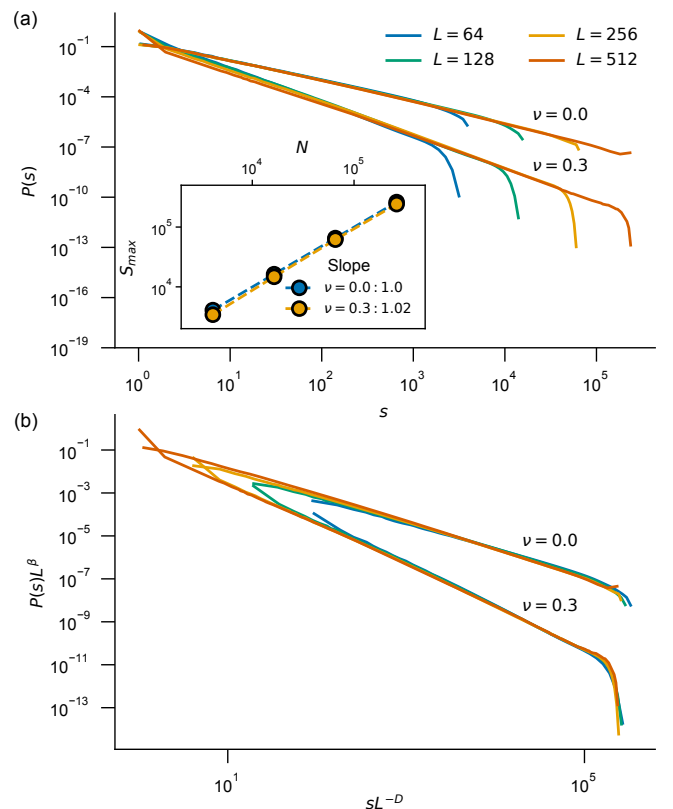


Figure 7. Size scaling in different regimes. (a), Avalanche size distribution in the OFC, model for different system sizes ($L = 64, 128, 256, 512$) and for two different dissipation values $\nu = 0$ and $\nu = 0.3$. In both regimes the cut-off values scale with the size of the system (inset). (b), Collapse of the distributions under finite-size scaling with $D = 2.2$ and $\beta = 4.2$ and 2.8 for $\nu = 0$ and $\nu = 0.3$ respectively.

equivalent measure of relative avalanche size. This proxy is commonly used in earthquake analogue experiments, including the granular fault experiments in Lyon [4] and the fracture experiments in Barcelona [11] (Fig. 1a). In the granular fault experiment in Rennes [5] (Fig. 1a), the seismic moment M_0 is measured directly. Finally, in the fracture experiment in Oslo [27] (Fig. 1a), the avalanche size s corresponds to the area of the clusters formed by the advance of the rupture front along the two-dimensional interface.

THEORETICAL DEVELOPMENT

Combining Eqs. (1) and (2) and the definition $d_{cp} \equiv 1/s_c$, we obtain

$$P(s|d_{cp}) = s^{-\tau_c} e^{-s/d_{cp}} / \mathcal{N} \quad (5)$$

where $\mathcal{N} = Ei(\tau_c, d_{cp})$ is a normalization constant for avalanche size $s \in [1, \infty)$.

The resulting avalanche distribution is

$$P(s) = \int_0^\infty P(s|d_{cp})P(d_{cp})d(d_{cp}) \quad (6a)$$

$$P(s) = s^{-\tau_c} \int_0^\infty e^{-s d_{cp}} d_{cp}^{-\gamma} \mathcal{L}(d_{cp})d(d_{cp}) \quad (6b)$$

with $\mathcal{L}(d_{cp}) \equiv L(d_{cp})/Ei(\tau_c, d_{cp})$. The integral in Eq.(6b) is the Laplace transform of $d_{cp}^{-\gamma} \mathcal{L}(d_{cp})$. Given the power-law behavior for $d_{cp} \rightarrow 0$ and the fact that $\mathcal{L}(d_{cp})$ is slowly varying at zero, Tauberian theorem indicates that the asymptotic behavior of $P(s)$ for large s is:

$$s \rightarrow \infty, P(s) \sim s^{-\tau}, \tau = \tau_c + 1 - \gamma > \tau_c \quad (7)$$

[1] B. Gutenberg and C. F. Richter, Magnitude and energy of earthquakes, *Ann. Geophys.* **9**, 1 (1956).

[2] P. Bak and C. Tang, Earthquakes as a self-organized critical phenomenon, *Journal of Geophysical Research: Solid Earth* **94**, 15635 (1989).

[3] H. Kawamura, T. Hatano, N. Kato, S. Biswas, and B. K. Chakrabarti, Statistical physics of fracture, friction, and earthquakes, *Rev. Mod. Phys.* **84**, 839 (2012).

[4] S. Lherminier, R. Planet, V. Levy dit Vehel, G. Simon, L. Vanel, K. J. Måløy, and O. Ramos, Continuously sheared granular matter reproduces in detail seismicity laws, *Phys. Rev. Lett.* **122**, 218501 (2019).

[5] D. Houdoux, A. Amon, D. Marsan, J. Weiss, and J. Crassous, Micro-slips in an experimental granular shear band replicate the spatiotemporal characteristics of natural earthquakes, *Communications Earth & Environment* **2**, 90 (2021).

[6] K. E. Daniels and N. W. Hayman, Force chains in seismogenic faults visualized with photoelastic granular shear experiments, *J. Geophys. Res. Solid Earth* **113**, 2156 (2008).

[7] A. Abed Zadeh, J. Barés, and R. P. Behringer, Crackling to periodic dynamics in granular media, *Phys. Rev. E* **99**, 040901 (2019).

[8] V. Frette, K. Christensen, A. Malthe-Sørensen, J. Feders, T. Jøssang, and P. Meakin, Avalanche dynamics in a pile of rice, *Nature* **379**, 49 (1996).

[9] O. Ramos, E. Altshuler, and K. J. Måløy, Avalanche prediction in a self-organized pile of beads, *Phys. Rev. Lett.* **102**, 078701 (2009).

[10] K. J. Måløy, S. Santucci, J. Schmittbuhl, and R. Toussaint, Local waiting time fluctuations along a randomly pinned crack front, *Phys. Rev. Lett.* **96**, 045501 (2006).

[11] Y. Xu, A. G. Borrego, A. Planes, X. Ding, and E. Vives, Criticality in failure under compression: Acoustic emission study of coal and charcoal with different microstructures, *Phys. Rev. E* **99**, 033001 (2019).

[12] J. Baró, Á. Corral, X. Illa, A. Planes, E. K. Salje, W. Schranz, D. E. Soto-Parra, and E. Vives, Statistical similarity between the compression of a porous material and earthquakes, *Phys. Rev. Lett.* **110**, 088702 (2013).

[13] M. Stojanova, S. Santucci, L. Vanel, and O. Ramos, High frequency monitoring reveals aftershocks in subcritical crack growth, *Phys. Rev. Lett.* **112**, 115502 (2014).

[14] J. Barés, A. Dubois, L. Hattali, D. Dalmas, and D. Bonamy, Aftershock sequences and seismic-like organization of acoustic events produced by a single propagating crack, *Nature Communications* **9**, 1253 (2018).

[15] P. Bak, C. Tang, and K. Wiesenfeld, Self-organized criticality: An explanation of the $1/f$ noise, *Phys. Rev. Lett.* **59**, 381 (1987).

[16] H. J. Jensen, *Self-organized Criticality, Emergent Complex Behavior in Physical and Biological Systems* (Cambridge Univ. Press, Cambridge, 1998).

[17] H. E. Stanley, *Introduction to Phase Transitions and Critical Phenomena* (Oxford Univ. Press, New York, 1987).

[18] P. Alstrøm, Mean-field exponents for self-organized critical phenomena, *Phys. Rev. A* **38**, 4905 (1988).

[19] K. Bækgaard Lauritsen, S. Zapperi, and H. E. Stanley, Self-organized branching processes: Avalanche models with dissipation, *Phys. Rev. E* **54**, 2483 (1996).

[20] S. Zapperi, K. B. Lauritsen, and H. E. Stanley, Self-organized branching processes: Mean-field theory for avalanches, *Phys. Rev. Lett.* **75**, 4071 (1995).

[21] P. Le Doussal and K. J. Wiese, Size distributions of shocks and static avalanches from the functional renormalization group, *Phys. Rev. E* **79**, 051106 (2009).

[22] D. Dhar and S. N. Majumdar, Abelian sandpile model on the bethe lattice, *Journal of Physics A: Mathematical and General* **23**, 4333 (1990).

[23] Y.-C. Zhang, Scaling theory of self-organized criticality, *Phys. Rev. Lett.* **63**, 470 (1989).

[24] S. Lübeck and K. D. Usadel, Numerical determination of the avalanche exponents of the bak-tang-wiesenfeld model, *Phys. Rev. E* **55**, 4095 (1997).

[25] A. Chessa, H. E. Stanley, A. Vespignani, and S. Zapperi, Universality in sandpiles, *Phys. Rev. E* **59**, R12 (1999).

[26] A. Vespignani, S. Zapperi, and L. Pietronero, Renormalization approach to the self-organized critical behavior of sandpile models, *Phys. Rev. E* **51**, 1711 (1995).

[27] K. J. Måløy, S. Santucci, J. Schmittbuhl, and R. Toussaint, Local waiting time fluctuations along a randomly pinned crack front, *Phys. Rev. Lett.* **96**, 045501 (2006).

[28] K. Duplat, G. Varas, and O. Ramos, Gutenberg-richter-like relations in physical systems (2025), arXiv:2512.17615 [cond-mat.stat-mech].

[29] V. Navas-Portella, A. González, I. Serra, E. Vives, and A. Corral, Universality of power-law exponents by means of maximum-likelihood estimation, *Phys. Rev. E* **100**, 062106 (2019).

[30] D. Dhar, The abelian sandpile and related models, *Physica A: Statistical Mechanics and its Applications* **263**, 4 (1999), proceedings of the 20th IUPAP International Conference on Statistical Physics.

[31] G. Ódor, Universality classes in nonequilibrium lattice systems, *Rev. Mod. Phys.* **76**, 663 (2004).

[32] R. J. Geller, D. D. Jackson, Y. Y. Kagan, and F. Mulargia, Earthquakes cannot be predicted, *Science* **275**, 1616 (1997).

[33] M. Wyss, Cannot earthquakes be predicted?, *Science* **278**, 487 (1997).

[34] I. Main, *Nature* (1999), <http://www.nature.com/nature/debates/earthquake/quakeframeset.html>.

[35] L. E. Aragón, E. A. Jagla, and A. Rosso, Seismic cycles, size of the largest events, and the avalanche size distribution in a model of seismicity, *Phys. Rev. E* **85**, 046112 (2012).

[36] L. E. Aragón and E. A. Jagla, Spatial and temporal forecasting of large earthquakes in a spring-block model of a fault, *Geophysical Journal International* **195**, 1763 (2013).

[37] E. A. Jagla, Forest-fire analogy to explain the b value of the Gutenberg-Richter law for earthquakes, *Phys. Rev. Lett.* **111**, 238501 (2013).

[38] M. Taroni and A. Akinci, Good practices in psha: declustering, b -value estimation, foreshocks and aftershocks inclusion; a case study in Italy, *Geophysical Journal International* **224**, 1174 (2020).

[39] Z. Olami, H. J. S. Feder, and K. Christensen, Self-organized criticality in a continuous, nonconservative cellular automaton modeling earthquakes, *Phys. Rev. Lett.* **68**, 1244 (1992).

[40] L. De Arcangelis, C. Godano, J. R. Grasso, and E. Lippiello, Statistical physics approach to earthquake occurrence and forecasting, *Physics Reports* **628**, 1 (2016).

[41] O. Ramos, E. Altshuler, and K. J. Måløy, Quasiperiodic events in an earthquake model, *Phys. Rev. Lett.* **96**, 098501 (2006).

[42] S. Pinho and C. Prado, Sequential updates for non-abelian SOC models, *The European Physical Journal B* **18**, 479 (2000).

[43] A. Corral, Long-term clustering, scaling, and universality in the temporal occurrence of earthquakes, *Phys. Rev. Lett.* **92**, 108501 (2004).

[44] E. Lippiello, L. de Arcangelis, and C. Godano, Memory in self-organized criticality, *Europhysics Letters* **72**, 678 (2005).

[45] P. Kumar, E. Korkolis, R. Benzi, D. Denisov, A. Niemeijer, P. Schall, F. Toschi, and J. Trampert, On interevent time distributions of avalanche dynamics, *Scientific Reports* **10**, 626 (2020).

[46] H. Kawamura, T. Yamamoto, T. Kotani, and H. Yoshino, Asperity characteristics of the Olami-Feder-Christensen model of earthquakes, *Phys. Rev. E* **81**, 031119 (2010).

[47] J. X. de Carvalho and C. P. C. Prado, Self-organized criticality in the Olami-Feder-Christensen model, *Phys. Rev. Lett.* **84**, 4006 (2000).

[48] J. A. Bonachela and M. A. Muñoz, Self-organization without conservation: true or just apparent scale-invariance?, *Journal of Statistical Mechanics: Theory and Experiment* **2009**, P09009 (2009).

[49] C. G. Sammis and D. Sornette, Positive feedback, memory, and the predictability of earthquakes, *Proceedings of the National Academy of Sciences* **99**, 2501 (2002).

[50] O. Ramos, Criticality in earthquakes. good or bad for prediction?, *Tectonophysics* **485**, 321 (2010).

[51] I. Main, Statistical physics, seismogenesis, and seismic hazard, *Reviews of Geophysics* **34**, 433 (1996).

[52] S. Lise and H. J. Jensen, Transitions in nonconserving models of self-organized criticality, *Phys. Rev. Lett.* **76**, 2326 (1996).

[53] D. S. Fisher, Collective transport in random media: from superconductors to earthquakes, *Physics Reports* **301**, 113 (1998).

[54] N. H. Sultan, K. Karimi, and J. Davidsen, Sheared granular matter and the empirical relations of seismicity, *Phys. Rev. E* **105**, 024901 (2022).

[55] K. A. Murphy, K. A. Dahmen, and H. M. Jaeger, Transforming mesoscale granular plasticity through particle shape, *Phys. Rev. X* **9**, 011014 (2019).

[56] A. Nicolas, E. E. Ferrero, K. Martens, and J.-L. Barrat, Deformation and flow of amorphous solids: Insights from elastoplastic models, *Rev. Mod. Phys.* **90**, 045006 (2018).

[57] D. Stauffer and A. Aharony, *Introduction To Percolation Theory* (CRC Press, 2003).

[58] G. L. Choy and J. L. Boatwright, Global patterns of radiated seismic energy and apparent stress, *J. Geophys. Res. Solid Earth* **100**, 18205 (1995).